Catalysis Today 165 (2011) 80–88

Contents lists available at ScienceDirect

Catalysis Today

journal homepage: www.elsevier.com/locate/cattod

# Density functional theory investigations on the catalytic mechanisms of hydrazine decompositions on Ir(1 1 1)

Ping-Xia Zhang[a], Yang-Gang Wang[a], Yan-Qiang Huang[b], Tao Zhang[b], Guo-Shi Wu[a], Jun Li[a,*]

[a] Department of Chemistry and Key Laboratory of Organic Optoelectronics and Molecular Engineering of Ministry of Education, Tsinghua University, Beijing 100084, China
[b] State Key Laboratory of Catalysis, Dalian Institute of Chemical Physics, Chinese Academy of Sciences, PO Box 110, Dalian 116023, China

ARTICLE INFO

*Article history:*
Received 8 October 2010
Received in revised form
30 December 2010
Accepted 9 January 2011
Available online 15 February 2011

*Keywords:*
Hydrazine
N–N cleavage
Decomposition mechanism
DFT calculations

ABSTRACT

The mechanisms of hydrazine decompositions on Ir(1 1 1) have been investigated by using slab model based on periodic density functional theory (DFT). In order to shed light on the elementary radical reaction processes of hydrazine decomposition on Ir-based catalysts, three possible reaction pathways are considered. Through computational modeling we have investigated the adsorption characteristics, geometrical structures, activation energies, and reaction mechanisms. The initial reactants, transition states, and final products of each elementary step and various likely intermediates are discussed. We have found that the main reaction channel with relatively low energy barriers is the following: the thermal decomposition of hydrazine forms two $NH_2$ radicals, which attack an adjacent adsorbed hydrazine molecule or subsequent $N_2H_x$ ($x = 1–3$) species and capture the H atoms step by step, finally leading to the formation of $N_2$ and $NH_3$ products. We show that the rate-determining step involves $NH_2$ interacting with a $N_2H$ species, with an energy barrier of 0.63 eV (or 14.5 kcal/mol). The overall reaction channel releases a large amount of thermal energies. The decomposition of hydrazine on Ir surfaces is therefore both thermodynamically and kinetically favorable. The other reaction channels investigated have much higher activation barriers with Ir catalysts.



## 1. Introduction

Hydrazine ($N_2H_4$) is an extraordinary energy material that has been widely involved in nuclear industry and aerospace science. The catalytic decomposition of $N_2H_4$ has stimulated strong interest in understanding the thermodynamics and kinetics because of its important applications in space technology—controlling and adjusting orbits and attitudes of satellites or spacecrafts. It is widely believed that hydrazine is decomposed with two typical reaction routes [1–3]:

$$N_2H_4 \rightarrow N_2 + 2H_2 \quad (R1)$$

$$3N_2H_4 \rightarrow N_2 + 4NH_3 \quad (R2)$$

In principle the newly formed $NH_3$ can decompose further at elevated temperatures, leading to eventual formation of dinitrogen and dihydrogen:

$$2NH_3 \rightarrow N_2 + 3H_2 \quad (R3)$$

Despite the latter reaction (R3) has rather high energy barriers in its elementary steps, this mechanism makes hydrazine as a promising compound for hydrogen storage and production. The whole reaction of hydrazine decomposition can be formulated as [4,5]:

$$3N_2H_4 \rightarrow 4(1-x)NH_3 + (1+2x)N_2 + 6xH_2 \quad (R4)$$

Here, $x$ denotes the selectivity of the catalyst toward $H_2$ production, which is the percentage of hydrazine decomposition via reaction (R1) or the percentage of the produced ammonia via decomposition reaction (R3). The specific reaction pathways depend on the nature of the catalysts and the reaction conditions, e.g., temperature and pressure [6].

A number of experimental works have been done on hydrazine decomposition. It turned out that the mechanisms of hydrazine decomposition are quite complicated and the exact pathways are not completely clear. Potential reaction pathways of hydrazine decomposition on metal surfaces were speculated based on various characterization techniques, including temperature programmed desorption (TPD), high resolution electron energy loss spectroscopy (HREELS), X-ray photoelectron spectroscopy (XPS), ultraviolet photoelectron spectroscopy (UPS), etc. Even with these efforts, the catalytic mechanisms of hydrazine decompositions are still controversial. Several possible radical channels were proposed. The decomposition of hydrazine was thought to take place mainly by the following two possible paths: (a) $N_2H_4$ undergoes intramolecular dehydrogenation by eliminating H atom one by one, finally resulting in the formation of the $N_2$ and $H_2$ products (R5), as have

* Corresponding author. Tel.: +86 10 62795381; fax: +86 10 62797472.
*E-mail address:* junli@tsinghua.edu.cn (J. Li).

0920-5861/$ – see front matter © 2011 Elsevier B.V. All rights reserved.
doi:10.1016/j.cattod.2011.01.012

been deduced from catalytic decomposition of hydrazine on surfaces of Ni(1 0 0) [7] and Pt(1 1 1) [8]; (b) the N–N bond of hydrazine cleaves firstly (R6), followed by further dehydrogenation of the newly formed $NH_2$ fragments into atomic N and H, and the latter recombine to form $N_2$ and $H_2$ molecules (R7). The formation of $N_2$ and $H_2$ is observed for catalytic decomposition on Fe(1 1 1) [6], transition metals (Cr, Mn, Fe, W, Re and Os) [9,10], polycrystalline aluminum [11], Ni(1 1 1) [12], polycrystalline iridium foil [13], and Pd(1 0 0) [14].

With different temperature or coverage of surface species, the specific reaction paths might be altered. For example, at low temperature path (a) seems to take place easily, whereas at high temperature path (b) seems favorable, as observed on Rh(1 1 1) [15], Si(1 1 1) [16] and polycrystalline rhodium surfaces [17]. Both decomposition paths is likely to proceed in parallel on Ru(0 0 1) surface [18]. Additionally, following the reaction (R6) the direct hydrogenation of $NH_2$ radical using the hydrogen produced from decomposed hydrazine may yield $NH_3$ molecules (R8) [6,9,15,19]. Beside these pathways, there are suggestions of other possible mechanisms. For example, the intramolecular proton transfer of hydrazine is thought to contribute to the formation of $NH_3$ (R9) on Rh(1 1 1) surface at low temperature [15]. The continuous hydrogenation of hydrazine might produce $NH_3$ (R10) on Pt(1 1 1) [8], tungsten film [10], and polycrystalline aluminum [11]. Adsorbed $N_2H_2$ intermediates might react with hydrazine molecules in the gas phase to give rise to $N_2$ and $NH_3$ molecules (R11) [13], etc.

$$N_2H_4(a) \rightarrow N_2H_3(a) + H(a) \rightarrow N_2H_2(a) + 2H(a) \rightarrow N_2H(a) + 3H(a) \rightarrow N_2(a) + 4H(a) \quad (R5)$$

$$N_2H_4(a) \rightarrow 2NH_2(a) \quad (R6)$$

$$NH_2(a) \rightarrow NH(a) + H(a) \rightarrow N(a) + 2H(a) \quad (R7)$$

$$NH_2(a) + H(a) \rightarrow NH_3(a) \quad (R8)$$

$$N_2H_4(a) \rightarrow NH_3(a) + NH(a) \quad (R9)$$

$$N_2H_4(a) + 2H(a) \rightarrow N_2H_5(a) + H(a) \rightarrow N_2H_6(a) \rightarrow 2NH_3(a) \quad (R10)$$

$$N_2H_2(a) + N_2H_4(g) \rightarrow N_4H_6(a) \rightarrow 2NH_3(a) + N_2(a) \quad (R11)$$

Here (*a*) and (*g*) represent the adsorbed and gas-phase species, respectively.

These experimental investigations have provided vital information about the catalytic reactions for the production of the three gaseous products ($NH_3$, $N_2$ and $H_2$) [19] by decomposition of hydrazine. Theoretical investigations are therefore needed to provide detailed understanding of the decomposition mechanisms, reaction dynamics, energy barriers, and the elementary steps. So far theoretical investigation on the mechanism of hydrazine decomposition on transition metal surfaces is rather scarce. No comprehensive computational study is performed on the mechanism of hydrazine decomposition, except a kinetic analysis of the catalytic decomposition of $N_2H_4$ by using the bond-order conservation-Morse potential (BOC-MP) method [20] and a recent density functional theory (DFT) calculation of hydrazine adsorption on Ni(1 0 0) surface [21]. We present here the first theoretical investigation for fundamental understanding of catalytic radical reaction processes of hydrazine decomposition on metal catalysts.

Currently, $Ir/Al_2O_3$ (20–40 wt%) is the commercial catalysts widely applied to the hydrazine decomposition in monopropellant thrusters [1]. Because iridium is rare and expensive, great effort is made to search for feasible high-performance substitutes for iridium catalysts [4,5,22–30]. However, none of them show better total performance than the conventional iridium catalyst. Understanding of the detailed elementary steps is essential for uncovering new catalysts with desired properties. Thus, we performed periodic DFT calculations of hydrazine decomposition on Ir substrate to elucidate the electronic structures and elementary reaction steps. In our calculations all the chemisorption and decomposition of hydrazine and related intermediates take place on the most stable Ir(1 1 1) plane. The adsorption geometries and energies, site preferences, relative stabilities of various species and reaction barriers are systematically characterized for possible channels. These studies aim at helping to design and develop new low-cost alternative materials with high durability and catalytic activity for the precious noble metal catalysts for hydrazine decompositions.

## 2. Computational methods

All the DFT calculations were performed by using DMol$^3$ program package (version 4.3) in the Materials Studio of Accelrys Inc [31,32]. The generalized gradient approximation (GGA) was employed with the Perdew–Burke–Ernzerhof (PBE) exchange-correlation functional [33]. We used localized double-numerical basis sets with polarization functions (DNP). For iridium atoms, the metal core electrons were replaced by the energy-consistent Stuttgart quasi-relativistic pseudopotentials (PP) of Andrae et al. [34], where the scalar-relativistic (mass–velocity and Darwin) effects are included. A Fermi smearing of 0.1 eV was used to improve the convergence of the self-consistent field calculations. We adopted a real-space cutoff of 4.2 Å and the convergence criteria of $4 \times 10^{-5}$ hartree, $4 \times 10^{-4}$ hartree/Å, and $5 \times 10^{-3}$ Å for energy, energy gradient and geometry, respectively. All the calculations were performed using the spin-polarized Kohn–Sham formalism. The calculated lattice constant for bulk iridium is 3.91 Å, which is in good agreement with the experimental value of 3.84 Å [35], indicating that the selected approach is adequate. The $6 \times 6 \times 1$ *k*-points grid was used for the surface brillouin zone integration. The Ir(1 1 1) surface was modeled by a four-layers periodic slab with a $4 \times 4$ unit-cell size and the images were separated by a vacuum-layer of 1 nm. During the geometry optimizations only the two top metal layers are relaxed to the lowest energy configurations. The complete LST/QST (the linear synchronous transit and quadratic synchronous transit) method was used to determine the transition states. In order to verify the validity of the transition states, the partial Hessian matrixes were calculated for all the intermediates related in the reactions and the several neighboring iridium atoms on the upmost surface. Previous theoretical results have shown that the results of the partial Hessian analyses are nearly the same as those of the full Hessian [36]. However, this approach obstructs the evaluation of the zero point energy (ZPE) for the correction of activation energies.

## 3. Results and discussion

### 3.1. Adsorption and structures of reaction intermediates on Ir(1 1 1)

The chemisorption properties for a series of intermediates in the reactions $N_2H_x$ ($x$ = 0–4), $NH_x$ ($x$ = 0–3) and H on Ir(1 1 1) are shown in Fig. 1 and Table 1, including geometrical parameters, adsorption preferences and adsorption energies. While numerous possible adsorption sites are explored, here only the stable adsorption sites are presented. We will present below the adsorption of various intermediate species on Ir(1 1 1) surfaces. The reaction barriers of the elementary steps will be discussed based on different adsorption modes and reaction pathways.

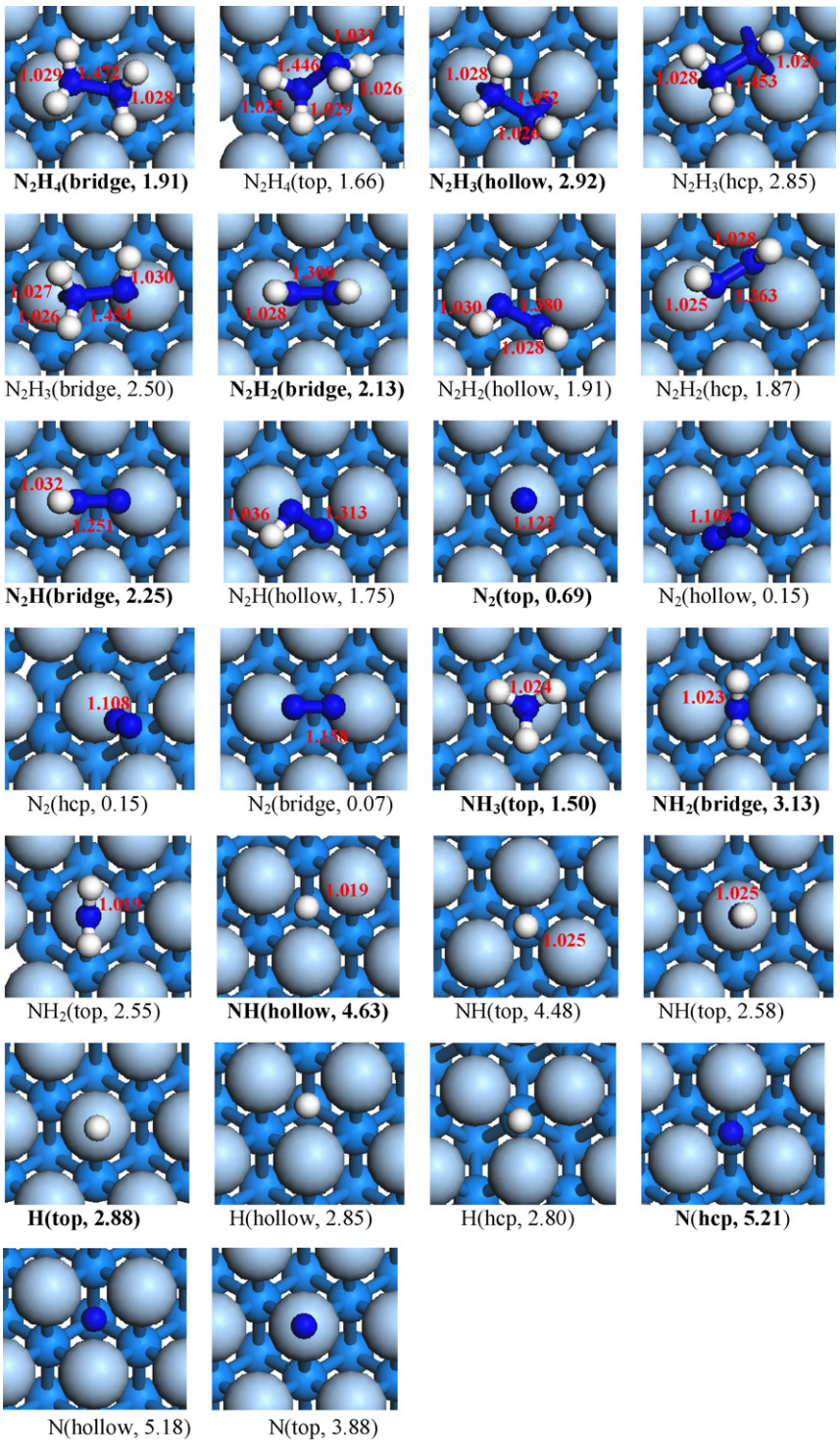


**Fig. 1.** Geometrical parameters (in Å) for adsorbed $N_2H_x$ ($x$ = 0–4), $NH_x$ ($x$ = 0–3) and H species on Ir(1 1 1) (top view). Adsorption sites and adsorption energies (eV) without ZPE correction are both given in parentheses. The most favorable site for each adsorbates and the corresponding adsorption energies are indicated in bold.

For $N_2H_4$, the bridge site is most stable, with the two nitrogen atoms bonded to the iridium surface. The corresponding adsorption energy is 1.91 eV, which is large enough to prevent desorption of the reactants. The non-bonding "lone pair" electrons on nitrogen atoms donate to the empty *d* orbitals of Ir atoms, leading to relative strong chemisorption. The $N_2H_4$ adsorbate has a structure with $C_2$ symmetry and the optimized N–N bond length is 1.472 Å and N–H bond lengths are 1.028 and 1.029 Å, respectively. In gas phase the gauche form with $C_2$ symmetry corresponds to the equilibrium conformation of hydrazine molecule [37,38]. In this structure the two $NH_2$ groups are rotated by approximately 90° with respect to each other to avoid repulsion of the lone-pairs. However, when hydrazine molecule adsorbs on Ir(1 1 1), the N–N bond is elongated and torsion of the $NH_2$ groups along the N–N bond becomes obviously smaller, approximately 30°, making it closer to the eclipsed conformation. The bonding between nitrogen and iridium atoms greatly decreases the intramolecular repulsive interaction of unshared non-bonding electron pairs on the N atoms of

**Table 1**
Adsorption energies (eV) for the different species on Ir(1 1 1).

| Species | Top | Bridge | Hollow | Hcp |
|---|---|---|---|---|
| $N_2H_4$ | 1.66 | 1.91 | – | – |
| $N_2H_3$ | – | 2.50 | 2.92 | 2.85 |
| $N_2H_2$ | – | 2.13 | 1.91 | 1.87 |
| $N_2H$ | – | 2.25 | 1.75 | |
| $N_2$ | 0.69 | 0.07 | 0.15 | 0.15 |
| $NH_3$ | 1.50 | – | – | – |
| $NH_2$ | 2.55 | 3.13 | – | – |
| NH | 2.58 | – | 4.63 | 4.48 |
| N | 3.88 | – | 5.18 | 5.21 |
| H | 2.88 | – | 2.85 | 2.80 |

hydrazine. When hydrazine adsorbs on the top site with N–N bond tilting on the surface, the torsion of $NH_2$ groups along the N–N bond is around 87° and the corresponding adsorption energy (1.66 eV) is lower than that of the bridge site. We have also investigated other possible modes of adsorptions and found that $N_2H_4$ prefers molecular adsorption on Ir(1 1 1), where a "side-on" adsorption mode with both nitrogen atoms bonded to the iridium atoms is more favorable than that of "end-on" adsorption mode with one nitrogen atom or two hydrogen atoms bonded to the surface.

The $N_2H_3$ fragment mainly has two types of preferred adsorption sites: (a) $N_2H_3$ lying on the bridge site with the N–N bond nearly parallel to the surface, (b) $N_2H_3$ sitting on the hollow-hole or hcp adsorption sites. For the later, the NH ends of $N_2H_3$ are much closer to the surface. When $N_2H_3$ fragment adsorbs on the hollow-hole site, the adsorption energy (2.92 eV) is the largest among all the possible adsorption modes, indicating that the hollow-site adsorption is energetically most favorable. Here $N_2H_3$ has a $C_s$-symmetry with N–N bond length of 1.452 Å, two N–H bonds of 1.028 Å, and the third N–H of 1.026 Å.

Similar to the $N_2H_3$ fragment, the diimide ($N_2H_2$) intermediate also has the identical site preferences. In the hollow-hole and hcp sites, the geometries of $N_2H_2$ are similar to each other, both lying on the surface. It is noteworthy to point out that the bridge site is most favorable for adsorption, with the largest adsorption energy of 2.13 eV. Here $N_2H_2$ has nearly $C_{2v}$ symmetry with the two H atoms far from the surface. The N–N bond length is 1.300 Å and two N–H bonds are 1.028 Å. $N_2H_2$ is an important intermediate during the hydrazine decomposition, which is observed as a gas-phase product from the Ni(1 0 0) surface in the 200–450 K [7].

For $N_2H$, the bridge site is again preferred, with an adsorption energy of 2.25 eV. The N–N bond length is 1.251 Å and N–H bond is 1.032 Å. For the hollow-hole site, $N_2H$ tilts toward the surface with a smaller adsorption energy (1.75 eV). We have tried to locate the $N_2H$ intermediate adsorbed on the hcp site, but it all leads to adsorption to other sites.

In the case of $N_2$, the top site is clearly preferred with the molecule axis perpendicular to the surface. The adsorption energy of this configuration is 0.69 eV and the N–N bond length is 1.123 Å (experimental values 1.098 Å [39]). For the bridge adsorption site, the adsorption energy of $N_2$ molecule is the lowest (0.07 eV). The N–N distance is 1.158 Å, while the distance between N and adjacent iridium atom is 2.196 Å. Obviously, the very stable $N_2$ molecule is easy to desorb from the surface. Rao et al. experimentally investigated the nature of the chemisorbed states of $N_2$ molecule on various transition metal surfaces (e.g., Ni, Fe, Cr, Ru, Re, W, etc.) and found that $N_2$ mainly has two chemisorbed states: "end-on" and "side-on". The former species has a bond order between 2.6 and 2.9, and the later between 1.4 and 2.0 [40]. This is consistent with the calculated N–N bond lengths, where the N–N distance in the top-adsorbed $N_2$ molecule is slightly shorter than that of the bridge-adsorbed one in our calculations. The $N_2$ molecule is also found to adsorb at the hollow-hole and hcp sites. The configuration of the hcp adsorption is similar to that of the hollow-hole adsorption, with a N–N bond length of 1.108 Å. Both have an adsorption energy of 0.15 eV, which is smaller than that of the top site. The $N_2$ adsorption at the hollow-hole and hcp locations were also found by Krekelberg et al. on Ir(1 1 1) by using both GGA-PW91 and RPBE functionals with DACAPO procedure [41].

The $NH_3$ adsorbate with $C_{3v}$ symmetry is chemisorbed molecularly on the surface via its N atom binding to a top site, due to the non-bonding "lone pair" of $NH_3$ strongly interacting with metal atom of the substrate. The optimized N–H bond length of 1.024 Å is consistent with the experimental result (1.021 Å) [39]. Here for $NH_3$ only the top site adsorption is favored, similar to $NH_3$ adsorption on Ir(1 0 0) [42].

Amide ($NH_2$) prefers to adsorb on the bridge site. The adsorption energy (3.13 eV) is rather large due to available valence at nitrogen atom. $NH_2$ has a $C_{2v}$ symmetry with two equal N–H bonds of 1.023 Å, comparable with the experimental value (1.024 Å) [39]. The $NH_2$ radical can also adsorb at top sites, but is energetically less stable than that of the bridge site. The same preference for $NH_2$ adsorption site was also found on Ir(1 0 0) [42].

The NH intermediate can adsorb on the top, hollow-hole and hcp sites. The corresponding adsorption energies are 2.58, 4.63 and 4.48 eV, respectively. Obviously, the hollow-hole site is the most stable site. The N–H bond lengths are 1.019 Å for top site and 1.025 Å for hollow-hole and hcp sites, respectively.

For the adatom H, three adsorption sites (top, hcp and hollow-hole) have the adsorption energies of 2.88, 2.85 and 2.80 eV, respectively, which are close to each other. The top-adsorbed H seems to be energetically the most favorable configuration, which is consistent with those found previously [41]. Interestingly, H is relatively mobile on the Ir(1 1 1) surface because of the lower diffusion barrier [41].

For the adsorbed N atom, the hcp adsorption site is preferred, with a binding energy of 5.21 eV, which is close to that (5.18 eV) of the hollow-hole-adsorbed configuration. We also find the top-adsorbed N atoms, which is less stable than those located at the hcp and hollow-hole sites.

It is interesting to compare the N–N bond lengths of $N_2H_x$ ($x$ = 0–4) adsorbates on the most favored binding sites. We find that upon adsorption the N–N distances decrease in the order of $N_2H_4 > N_2H_3 > N_2H_2 > N_2H > N_2$, indicating that the abstraction of hydrogen atoms from $N_2H_4$ and subsequent dehydrogenated species results in the strengthening of N–N bonds step by step.

### 3.2. Reaction pathways for $N_2H_4$ decomposition

#### 3.2.1. Intramolecular dehydrogenation of $N_2H_4$

From experiments on the catalytic decomposition of $N^{15}$-labeled hydrazine on alumina supported metals in the temperature range 333–573 K [2] and on the MgO-supported iron at low temperature [43] it is concluded that $N_2$ molecule originates from the same hydrazine molecule. Previous experiments [7,8,15–17] seem to suggest that the gradual intramolecular dehydrogenation of $N_2H_4$ leads to the formation of $N_2$. To a certain degree the experimental finding of the existence of diimide ($N_2H_2$) intermediates from thermal desorption spectra on the Ni(1 0 0) surface [7] seems to support this pathway. Thus, we firstly investigate the stepwise dehydrogenation process of hydrazine on Ir(1 1 1) surface. The stepwise dissociations of hydrazine to $N_2H_x$ ($x$ = 3–0) and dissociative hydrogen adatoms are considered, as shown in reaction (R5). During the calculations, we allow hydrogen atoms to diffuse far enough from the nitrogen-containing species $N_2H_x$ ($x$ = 1–3) to avoid the reversed hydrogenation reactions. The transition states for the elementary steps are depicted in Fig. 2 and the reaction energies are also shown in Fig. 3 to illustrate the relative stabilities of species involved in the dehydrogenation of $N_2H_4$.

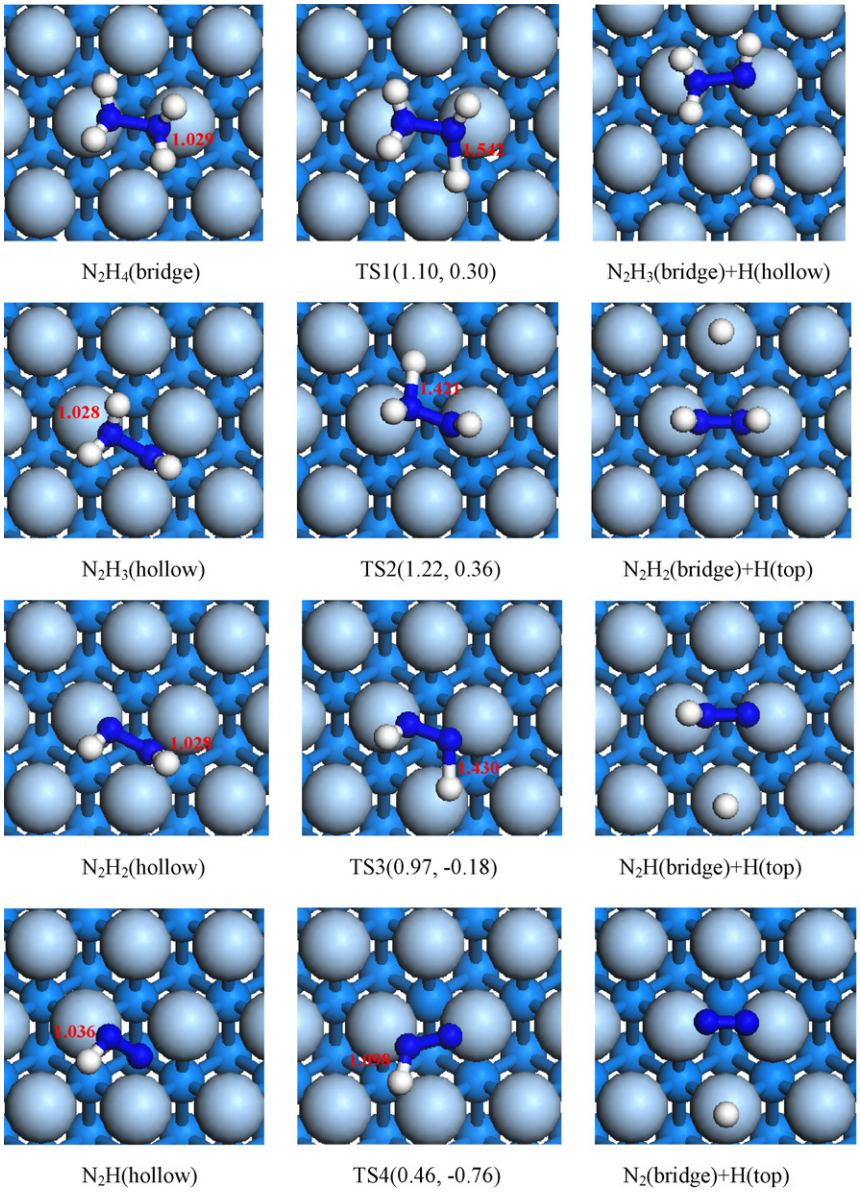


**Fig. 2.** The initial, transition and final states for dehydrogenation processes of adsorbed hydrazine (top view). Reaction barrier ($E_{rea}$) and energy change ($\Delta E$) in eV are given in brackets. TS denotes the transition state. The critical N–H bond lengths for reactants and transition states are given in Å.

As shown in Fig. 2, for the first hydrogen abstraction process, the $N_2H_4$ adsorbed on a bridge site is taken as the initial state. For the final state, $N_2H_3$ still lies at the bridge site while hydrogen moves directly from its initial position on the hydrazine molecule to the adjacent hollow-hole location. The energy barrier is 1.10 eV and the reaction is endothermic by 0.30 eV. For the transition state, the N–H bond length is about 1.542 Å and the imaginary frequency is $961i\,cm^{-1}$, corresponding to the N–H bond stretching. As expected, the energy barrier of N–H bond cracking of hydrazine is much higher than that of N–N bond on the iridium catalyst (see Fig. 4), indicating that the dissociation of N–H bond of hydrazine on Ir(1 1 1) is more difficult than of the N–N bond. We also find that the $N_2H_3$ intermediate can easily diffuse from the bridge site to the most stable hollow-hole site, with a small energy barrier of 0.13 eV and a large exothermicity of 0.42 eV (Table 2).

Subsequent intramolecular dehydrogenation reaction of $N_2H_3$ can lead to the formation of diimide ($N_2H_2$) and hydrogen adatom. The reactant $N_2H_3$ prefers to adsorb on a hollow-hole site, while in the products $N_2H_2$ migrates to the bridge site and H atom diffuses to the top position. For this path, the energy barrier is 1.22 eV and the endothermic energy is 0.36 eV. The transition state indeed possesses one large imaginary frequency ($1222i\,cm^{-1}$).

**Table 2**
The diffusion barriers ($E_{dif}$), energy change ($\Delta E$) and imaginary frequencies ($\nu$) of the transition states for the diffusions of some $N_2H_x$ ($x$ = 0–3) species adsorbed on Ir(1 1 1).

| Adsorbates | | $E_{dif}$ (eV) | $\Delta E$ (eV) | $\nu$ ($cm^{-1}$) |
|---|---|---|---|---|
| $N_2H_3$ | Bridge → hollow | 0.13 | −0.42 | 183$i$ |
| $N_2H_2$ | Hollow → bridge | 0.08 | −0.22 | 199$i$ |
| $N_2H$ | Hollow → bridge | 0.19 | −0.51 | 325$i$ |
| $N_2$ | Bridge → top | 0.04 | −0.76 | 150$i$ |

For the third step, the produced $N_2H_2$ fragment diffuses firstly from a bridge site to a slightly higher energy hollow site (Fig. 3), which has a barrier of 0.30 eV (Table 2). Therefore, in the subsequent reactions, $N_2H_2$ is located near the hollow-hole site as the initial state, which upon dehydrogenation generates $N_2H$ interme-

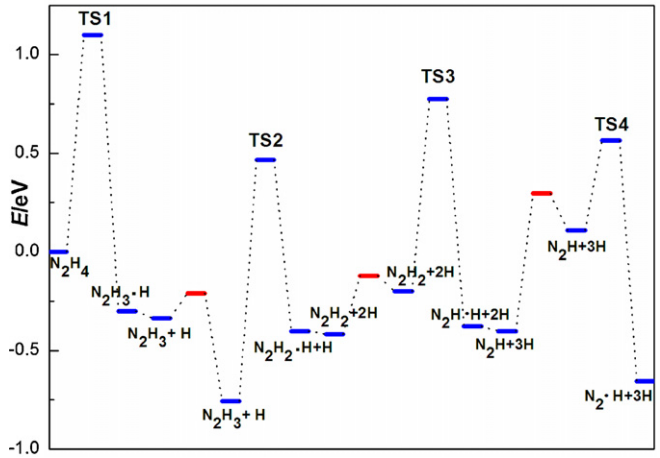


**Fig. 3.** A schematic illustration of the energetics of the hydrazine dehydrogenation pathway. The red bars represent transition states for diffusion of $N_2H_x$ ($x$ = 1–3) species (see Table 2). (For interpretation of the references to color in this figure legend, the reader is referred to the web version of the article.)

diate sitting at the bridge site with its molecular axis nearly parallel to the surface and H adatoms moving to the nearest top position. From our calculations, the energy barrier is 0.97 eV and the reaction is exothermic by 0.18 eV. The transition state is identified by an imaginary frequency of 1227$i$ cm$^{-1}$, corresponding to the N–H stretching vibration.

In the fourth step, further dehydrogenation of the $N_2H$ intermediate causes the complete scission of the N–H bonds, which forms $N_2$ molecule and adsorbed atomic hydrogen atom. The initial state is taken as a hollow-hole-adsorbed $N_2H$ radical, and the final state is taken as bridge-adsorbed $N_2$ molecule and top-adsorbed H. The reaction is exothermic by 0.76 eV and the energy barrier is 0.46 eV. The imaginary frequency of the transition state is 140$i$ cm$^{-1}$. Before the last dehydrogenation step, $N_2H$ fragment firstly diffuses in reversed direction to a slightly high energy hollow-hole site with a barrier of 0.19 eV (Table 2), which makes the subsequent reaction to occur very easily (Fig. 3). Obviously, the stepwise intramolecular dehydrogenation of hydrazine to form $N_2$ and $H_2$ is not a fast process at low temperature due to the relatively high energy barriers.

### 3.2.2. *Intramolecular dehydrogenation with N–N bond cleavage*

Inasmuch as the N–N bond energy (≈2.60 eV) of hydrazine is much lower than that of the N–H bond (3.60 eV) [43], hydrazine is expected to easily dissociate via N–N bond cleavage to form adsorbed amide radicals ($NH_2$) on Ir(1 1 1). This is supported by our present theoretical investigation on various reaction pathways. We take the most stable configuration of $N_2H_4$ adsorbed on the bridge site as the initial state, and two $NH_2$ products both adsorbed on the bridge site as the final state, as shown in Fig. 4. The reaction energy barrier is only 0.52 eV for N–N cleavage of hydrazine and the exothermic energy is about 0.93 eV, indicating that the dissociation of the N–N bond is energetically feasible in low temperature. This N–N bond cleavage channel of $N_2H_4$ decomposition is reminiscent to the thermal decomposition of ammonia borane

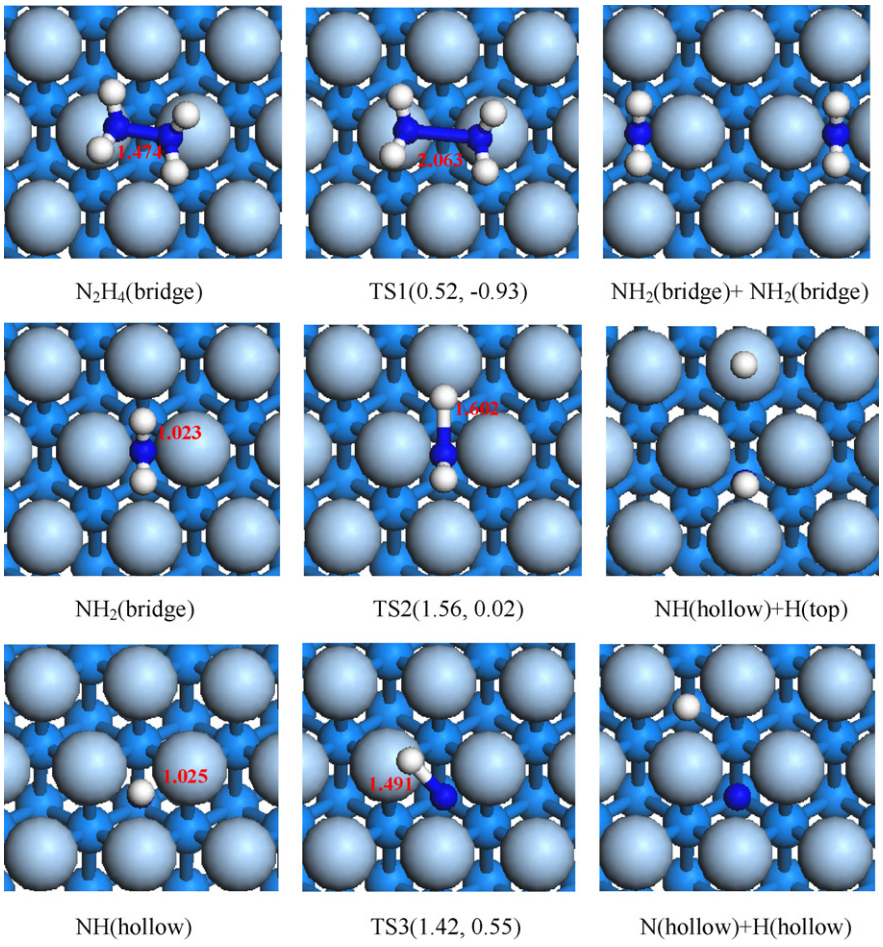


**Fig. 4.** The reactants, transition states (TS) and products for N–N bond cleavage of adsorbed hydrazine and the dehydrogenation of $NH_2$ radical (top view). Reaction barrier ($E_{rea}$) and energy change ($\Delta E$) in eV are listed in parentheses. Selected N–N and N–H bond lengths of the reactants and TS states are listed in Å.

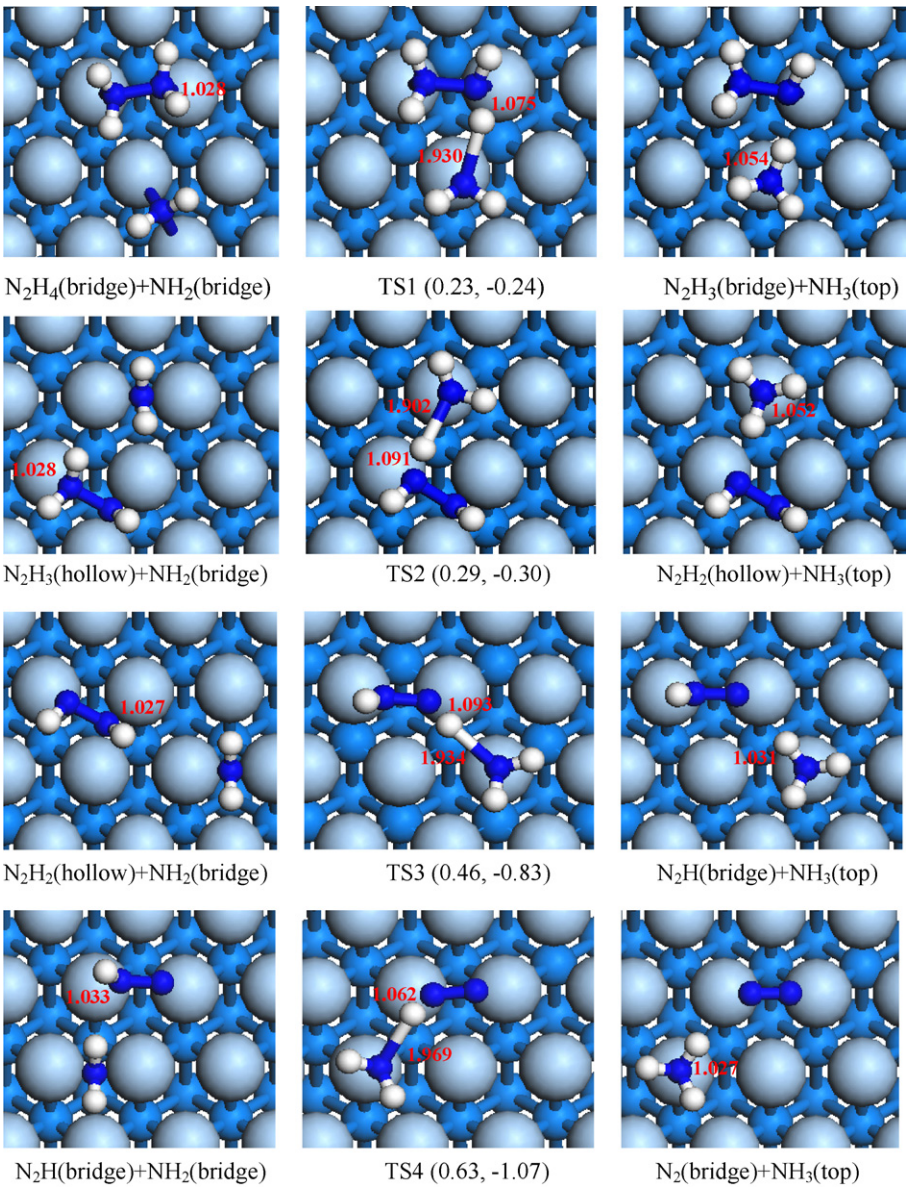


**Fig. 5.** Structures of the reactants, transition states, and products for the $NH_2$ abstracting the hydrogen atoms of $N_2H_x$ ($x$ = 4–1) on Ir(1 1 1) (top view). TS denotes the transition state. Reaction barrier ($E_{rea}$) and energy change ($\Delta E$) in eV are given in parentheses. Selected N–H bond distances for the reactants, TS states and products are shown in Å.

($NH_3BH_3$), in which the B–N bond cleavage plays a significant role in the dehydrogenation and formation of oligomers [44].

The $NH_2$ species from the cleavage of hydrazine N–N bond on Ir(1 1 1) can either attack another $N_2H_4$ molecule through an intermolecular mechanism or further undergo an intramolecular dehydrogenation. The intramolecular dehydrogenation of $NH_2$ seems to be rather difficult based on the calculated barriers for ammonia decomposition. Theoretical investigation of the decomposition of $NH_3$ on the Ir(1 0 0) indicates that without ZPE correction the energy barriers for the reactions $NH_3(a) \rightarrow NH_2(a) + H(a)$, $NH_2(a) \rightarrow NH(a) + H(a)$ and $NH(a) \rightarrow N(a) + H(a)$ are 1.14, 1.29 and 1.04 eV, respectively, based on VASP calculations [42]. In our PBE calculations with DMol$^3$, the energy barriers of $NH_2(a) \rightarrow NH(a) + H(a)$ and $NH(a) \rightarrow N(a) + H(a)$ on Ir(1 1 1) are 1.56 and 1.42 eV, as depicted in Fig. 4. The calculated imaginary frequencies are 1299$i$ and 1219$i$ cm$^{-1}$, respectively. Although the direct decomposition of $NH_2$ to NH as well as adsorbed N and H atoms is considered as a part of $NH_3$ decomposition on iridium catalyst, the high energy barriers of intramolecular $NH_2$ dehydrogenation show that these two steps are difficult to proceed. Other pathways must be responsible for the facile decomposition of hydrazine at room temperature.

### 3.2.3. *Intermolecular hydrogen abstraction via $NH_2$ attacking $N_2H_4$*

From experiments the products of hydrazine decomposition over 31.6 wt% $Ir/Al_2O_3$ catalyst surface change with the temperature. Blow 573 K the main product includes $N_2$ and $NH_3$, and between 573 K and 723 K a mixture of $N_2$, $NH_3$ and $H_2$ are observed, while above 723 K only $N_2$ and $H_2$ are detected [4]. Recently, it has been shown that at room temperature the Rh nanoparticles are highly active in catalyzing hydrous hydrazine decomposition toward $N_2$ and $H_2$ [45] demonstrated above, at low temperature the dehydrogenation of $NH_2$ to yield atomic N and its recombined $N_2$ molecule is rather difficult. Other possible dissociation pathway needs to be explored.

Experimentally catalytic decomposition of hydrazine occurs fast and acutely with Ir catalysts, which forms the basis for using the decomposition products as propellants for satellite rocket engines. Indeed Sawin and Merrill observed the emission of nitrogen prod-

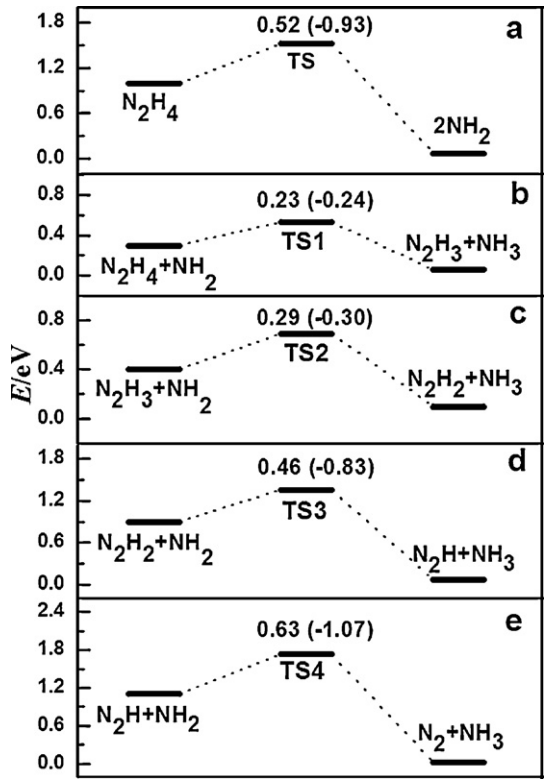


**Fig. 6.** The reaction barriers and the energy change of the reactions (in parentheses) for the reactions of (a) N–N bond cleavage of adsorbed hydrazine and (b–e) successive intermolecular reactions of $NH_2$ attacking $N_2H_x$ ($x$ = 4–1) on Ir(1 1 1). All energies are in eV.

uct at the temperature as low as 290 K from the temperature programmed decomposition (TPD) of hydrazine on Ir(1 1 1) [46]. The two catalytic paths discussed above for the heterogeneous decomposition of $N_2H_4$ are thus not possible at low temperature due to the high energy barriers of transition states. As we show earlier, the N–N bond of hydrazine is easy to break to form $NH_2$ radicals on the Ir(1 1 1) surface. It is therefore possible that the $NH_2$ radical can react with another $N_2H_4$ to abstract hydrogen atoms from the latter step by step. We therefore propose the following multi-step reaction mechanism for producing $N_2$ and $NH_3$ on Ir(1 1 1) surface.

$$N_2H_4(a) \overset{+NH_2(a)}{\longrightarrow} N_2H_3(a) + NH_3(a) \overset{+NH_2(a)}{\longrightarrow} N_2H_2(a) + 2NH_3(a) \overset{+NH_2(a)}{\longrightarrow} N_2H(a) + 3NH_3(a) \overset{+NH_2(a)}{\longrightarrow} N_2(a) + 4NH_3(a) \quad \text{(R12)}$$

The initial, transition and final states involved in each elementary steps of this mechanism are shown in Fig. 5, where the changes of reaction energies and the geometrical parameters are also shown. The transition state energies and reaction energies for the reactions of the N–N bond cleavage of adsorbed hydrazine (a) and successive intermolecular reactions of $NH_2$ attacking $N_2H_x$ ($x$ = 4–1) (b–e) on Ir(1 1 1) are shown in Fig. 6. As the first hydrogen atom is abstracted from the adsorbed hydrazine by $NH_2$ radical, $N_2H_3$ intermediate ends up in a bridge site and the $NH_3$ molecule adsorbs on the neighboring top site. For the transition state, the N–H bond length is of 1.93 Å and the imaginary frequency is $200i\,cm^{-1}$. The reaction barrier for this reaction step is only 0.23 eV, and the corresponding exothermic energy is 0.24 eV. After $NH_3$ molecule desorbs from surface, the $N_2H_3$ intermediate can easily diffuse from the bridge site to the most stable hollow-hole site with a small energy barrier of 0.13 eV and exothermic energy change of 0.42 eV (Table 2).

**Table 3**
The reaction barriers ($E_{rea}$), energy change ($\Delta E$) and imaginary frequencies ($\nu$) of the transition states for some intramolecular and intermolecular reactions on Ir(1 1 1).

| Reactions | $E_{rea}$ (eV) | $\Delta E$ (eV) | $\nu$ ($cm^{-1}$) |
|---|---|---|---|
| $N_2H_4 \rightarrow N_2H_3 + H$ | 1.10 | 0.30 | $961i$ |
| $N_2H_3 \rightarrow N_2H_2 + H$ | 1.22 | 0.36 | $1222i$ |
| $N_2H_2 \rightarrow N_2H + H$ | 0.97 | −0.18 | $1227i$ |
| $N_2H \rightarrow N_2 + H$ | 0.46 | −0.76 | $140i$ |
| $N_2H_4 \rightarrow NH_2 + NH_2$ | 0.52 | −0.93 | $242i$ |
| $NH_2 \rightarrow NH + H$ | 1.56 | 0.02 | $1299i$ |
| $NH \rightarrow N + H$ | 1.42 | 0.55 | $1219i$ |
| $N_2H_4 + NH_2 \rightarrow N_2H_3 + NH_3$ | 0.23 | −0.24 | $200i$ |
| $N_2H_3 + NH_2 \rightarrow N_2H_2 + NH_3$ | 0.29 | −0.30 | $136i$ |
| $N_2H_2 + NH_2 \rightarrow N_2H + NH_3$ | 0.46 | −0.83 | $161i$ |
| $N_2H + NH_2 \rightarrow N_2 + NH_3$ | 0.63 | −1.07 | $445i$ |

In the second step, the $N_2H_3$ intermediate can react with the second $NH_2$ radical to yield $NH_3$ and diimide ($N_2H_2$). The hollow-hole and bridge sites are preferred for adsorption of $N_2H_3$ and $NH_2$, respectively, while $N_2H_2$ prefers the hollow-hole and $NH_3$ the top sites. From the transition state search, the transition state has an imaginary frequency of $136i\,cm^{-1}$ and the reaction barrier for this reaction step is as low as 0.29 eV, with a reaction exothermic energy change of 0.30 eV.

In the third step, the $NH_2$ radical adsorbed at a bridge site interacts with the $N_2H_2$ fragment adsorbed at the hollow-hole site, leading to the formation of $N_2H$ species at a bridge site and $NH_3$ at a top site. This process is exothermic by 0.83 eV. The transition state has an energy barrier of 0.46 eV and an imaginary frequency of $161i\,cm^{-1}$.

In the final step, $N_2H$ and $NH_2$ radical will react to break the last N–H bond, leading to formation of molecular dinitrogen and ammonia. Here $N_2H$ and $NH_2$ can co-adsorb at the bridge sites, and the reaction products $N_2$ and $NH_3$ prefer adsorption at the bridge and top sites, respectively. The transition state has an imaginary frequency of $445i\,cm^{-1}$ and the reaction barrier is 0.63 eV. This final step is highly exothermic, with a calculated energy change of 1.07 eV. The $N_2$ molecule produced can either desorb from the catalyst surface due to the low adsorption energy (see Fig. 1) or diffuse to the more stable top site with a low barrier of 0.04 eV and a large exothermic energy of 0.76 eV (see Table 2).

From our calculations, once amide radical ($NH_2$) is formed all the elementary reaction steps are fairly easy without dissociation of the N–N bond in the whole process. This mechanism for the formation of $NH_3$ and $N_2$ is consistent with the experimental results of Aika et al. [47], where $NH_2$ seemed to play an important role in the decomposition of hydrazine. The necessity to have enough $NH_2$ radical to start the chain reactions explains the *induction period* [48,49] observed in the kinetics of hydrazine decomposition.

### 3.3. Discussion of the reaction pathways

From Table 3, the energy barrier of the rate-determining step for the intramolecular dehydrogenation of hydrazine (R5) is relatively high, about 1.22 eV for $N_2H_3(hollow) \rightarrow N_2H_2(bridge) + H(top)$. Both reactions (R5) and (R7) have high energy barrier. However, for the amide radical mechanism (R12) the activation energy of the rate-determining step ($N_2H + NH_2 \rightarrow N_2 + NH_3$) is only 0.63 eV. One can conclude that this latter reaction pathway is most likely the major mechanism for $N_2H_4$ decomposition in Ir(1 1 1) surface. Indeed hydrazine decomposition can be explosive when $N_2H_4$ is exposed to a metal catalyst. The reaction pathway (R12) results in the formation of $N_2$ without rupture of the N–N bond in $N_2H_4$. All the elementary steps are exothermic and have relatively low energy barriers, making this process being feasible at low temperature. It is almost a chain reaction upon formation of the $NH_2$ radical. This

mechanism agrees well with the experimental observation that the N–N bond remains intact during hydrazine decomposition [2,43].

It is known that the desorption and dissociation of $NH_3$ on Ir(1 0 0) is competitive [42–50]. At low temperature desorption of $NH_3$ is more notable, whereas with the elevation of temperature the decomposition of $NH_3$ becomes more plausible. From our calculations with the Ir(1 1 1) surface, the produced $NH_3$ molecules mostly desorb at the low temperature. At higher temperature $NH_3$ can further decompose to form atomic H and N, the recombination of which can lead to the formation of $N_2$ and $H_2$ molecules.

In summary, at low temperature hydrazine decomposition on Ir(1 1 1) first yields $NH_3$ and $N_2$, while at higher temperature $H_2$ is also formed. For the whole process of hydrazine decomposition on Ir(1 1 1), the most favorable mechanism is that $NH_2$ radicals firstly interact with the hydrogen atoms of the adsorbed $N_2H_4$ molecule and subsequent fragments $N_2H_x$ ($x$ = 1–3), leading to formation of $NH_3$ and $N_2$. As temperature elevating, the produced $NH_3$ will further decompose to produce $H_2$. When the temperature is high enough, all $NH_3$ is decomposed, leading to $N_2$ and $H_2$ as the only products. At high temperature the intramolecular dehydrogenation of $N_2H_4$ or the $NH_2$ product may also become possible, resulting in the formation of $N_2$ and $H_2$.

It is worth mentioning that while hydrazine decomposition leads to $NH_3 + N_2$ on Ir surfaces, $N_2H_4 \rightarrow N_2 + H_2$ pathway is more favorable at Ni surface or Ni–M alloys. Experimentally it is found that the $H_2$ selectivity can reach more than 90% at 30–40 °C on $Ni/SiO_2$ catalyst for hydrazine decomposition [26]. Additionally, by doping small amount of Ir or Pt, e.g. in bimetallic $Ni_{0.95}Ir_{0.05}$ and $Ni_{0.93}Pt_{0.07}$ alloy nanocatalysts, $H_2$ selectivity can be enhanced to 100% at room temperature [29,51]. Theoretical investigations of the mechanisms of hydrazine decomposition on Ni and NiM alloys are ongoing in our laboratory.

## 4. Conclusions

In this paper, periodic DFT calculations have been performed to investigate the reaction mechanism of hydrazine ($N_2H_4$) decomposition on Ir(1 1 1) surface. We have examined the processes of intramolecular and intermolecular $N_2H_4$ dehydrogenation. The calculated energetics show that on Ir(1 1 1) surfaces it is unlikely to produce a large amount of $N_2$ through intramolecular dehydrogenation at low temperature due to the relatively high activation barriers. Instead, because the intramolecular N–N bond cleavage of hydrazine is easier to take place than that of N–H bond, amide radicals ($NH_2$) can be formed on Ir(1 1 1). These radicals can abstract the hydrogen atoms of $N_2H_4$ or its products one by one, leading to the formation of $N_2$ and $NH_3$ molecules. The rate-determining step, where $NH_2$ radical reacts with $N_2H$ fragment, has an energy barrier of 0.63 eV. Our calculations indicate that the overall decomposition reaction is highly exothermic and the intermolecular mechanism is kinetically more favorable than any intramolecular mechanisms. Our results provide theoretical insight for understanding the catalytic decomposition mechanism of hydrazine on Ir(1 1 1) and other metal surfaces.

## Acknowledgements

The authors are grateful to Professors Qingfeng Ge and Qiang Xu for helpful discussions. This work was supported by NKBRSF (2011CB932400) and NSFC (20933003, 11079006, 91026003) of China. The calculations were performed by using supercomputers at the Computer Network Information Center, Chinese Academy of Sciences, the Shanghai Supercomputing Center, and Tsinghua National Laboratory for Information Science and Technology.

## References

[1] J.P. Contour, G. Pannetier, J. Catal. 24 (1972) 434–445.
[2] R. Maurel, J.C. Menezo, J. Catal. 51 (1978) 293–295.
[3] D.G. Tong, X.L. Zeng, W. Chu, D. Wang, P. Wu, Mater. Res. Bull. 45 (2010) 442–447.
[4] X. Chen, T. Zhang, M. Zheng, Z. Wu, W. Wu, C. Li, J. Catal. 224 (2004) 473–478.
[5] M. Zheng, X. Chen, R. Cheng, N. Li, J. Sun, X. Wang, T. Zhang, Catal. Commun. 7 (2006) 187–191.
[6] M. Grunze, Surf. Sci. 81 (1979) 603–625.
[7] S.X. Huang, T.S. Rufael, J.L. Gland, Surf. Sci. Lett. 290 (1993) L673–L676.
[8] D.J. Alberas, J. Kiss, Z.-M. Liu, J.M. White, Surf. Sci. 278 (1992) 51–61.
[9] V.J. Völter, G. Lietz, Z. Anorg. Chem. Bd. 366 (1969) 191–200.
[10] R.C. Cosser, F.C. Tompkins, Trans. Faraday Soc. 67 (1971) 526–544.
[11] D.W. Johnson, M.W. Roberts, J. Electron Spectrosc. Relat. Phenom. 19 (1980) 185–195.
[12] J.L. Gland, G.B. Fisher, G.E. Mitchell, Chem. Phys. Lett. 119 (1985) 89–92.
[13] B.J. Wood, H. Wise, J. Catal. 39 (1975) 471–480.
[14] R. Dopheide, L. Schröter, H. Zacharias, Surf. Sci. 257 (1991) 86–96.
[15] M.L. Wagner, L.D. Schmidt, Surf. Sci. 257 (1991) 113–128.
[16] Y. Bu, D.W. Shinn, M.C. Lin, Surf. Sci. 276 (1992) 184–199.
[17] J. Prasad, J.L. Gland, Surf. Sci. 258 (1991) 67–74.
[18] H. Rauscher, K.L. Kostov, D. Menzel, Chem. Phys. 177 (1993) 473–496.
[19] J.L. Falconer, H. Wise, J. Catal. 43 (1976) 220–233.
[20] J.E. de Medeiros, G.P. Valença, Braz. J. Chem. Eng. 15 (1998) 126.
[21] M.K. Agusta, M. David, H. Nakanishi, H. Kasai, Surf. Sci. 604 (2010) 245–251.
[22] X. Chen, T. Zhang, P. Ying, M. Zheng, W. Wu, L. Xia, T. Li, X. Wang, C. Li, Chem. Commun. 3 (2002) 288–289.
[23] R. Cheng, Y. Shu, M. Zheng, L. Li, J. Sun, X. Wang, T. Zhang, J. Catal. 249 (2007) 397–400.
[24] J. Sun, M. Zheng, X. Wang, A. Wang, R. Cheng, T. Li, T. Zhang, Catal. Lett. 123 (2008) 150–155.
[25] H. Wang, A. Wang, X. Wang, T. Zhang, Chem. Commun. (2008) 2565–2567.
[26] M. Zheng, R. Cheng, X. Chen, N. Li, L. Li, X. Wang, T. Zhang, Int. J. Hydrogen Energy 30 (2005) 1081–1089.
[27] L. Ding, Y. Shu, A. Wang, M. Zheng, L. Li, X. Wang, T. Zhang, Appl. Catal. A: Gen. 328 (2007) 58–67.
[28] S.K. Singh, Q. Xu, J. Am. Chem. Soc. 131 (2009) 18032–18033.
[29] S.K. Singh, Q. Xu, Inorg. Chem. 49 (2010) 6148–6152.
[30] J.B.O. Santos, G.P. Valença, J.A.J. Rodrigues, J. Catal. 210 (2002) 1–6.
[31] B. Delley, J. Chem. Phys. 92 (1990) 508–517.
[32] B. Delley, J. Chem. Phys. 113 (2000) 7756–7764.
[33] J.P. Perdew, K. Burke, M. Ernzerhof, Phys. Rev. Lett. 77 (1996) 3865–3868.
[34] D. Andrae, U. Häußermann, M. Dolg, H. Stoll, H. Preuß, Theor. Chim. Acta 77 (1990) 123–141.
[35] C. Kittel, Introduction to Solid State Physics, Wiley, New York, 1996.
[36] H. Orita, K. Uchida, N. Itoh, J. Mol. Catal. A 193 (2003) 197–205.
[37] J.O. Jarvie, A. Rauk, Can. J. Chem. 52 (1974) 2785–2791.
[38] J.A. Pople, L.A. Curtiss, J. Chem. Phys. 95 (1991) 4385–4388.
[39] D.R. Lide, CRC Handbook of Chemistry and Physics, CRC Press, New York, 1996.
[40] C.N.R. Rao, G.R. Rao, Surf. Sci. Rep. 13 (1991) 221–263.
[41] W.P. Krekelberg, J. Greeley, M. Mavrikakis, J. Phys. Chem. B 108 (2004) 987–994.
[42] W. Huang, W. Lai, D. Xie, Surf. Sci. 602 (2008) 1288–1294.
[43] J. Block, G. Schulz-Ekloff, J. Catal. 30 (1973) 327–329.
[44] J. Li, S.M. Kathmann, H.S. Hu, G.K. Schenter, T. Autrey, M. Gutowski, Inorg. Chem. 49 (2010) 7710–7720.
[45] S.K. Singh, X.B. Zhang, Q. Xu, J. Am. Chem. Soc. 131 (2009) 9894–9895.
[46] H.H. Sawin, R.P. Merrill, J. Chem. Phys. 73 (1980) 996–998.
[47] K.I. Aika, T. Ohhata, A. Ozaki, J. Catal. 19 (1970) 140–143.
[48] A.A. Konnov, J. De Ruyck, Combust. Flame 124 (2001) 106–126.
[49] X. Chen, T. Zhang, L. Xia, T. Li, M. Zheng, Z. Wu, X. Wang, Z. Wei, Q. Xin, C. Li, Catal. Lett. 79 (2002) 21–25.
[50] A.K. Santra, B.K. Min, C.W. Yi, K. Luo, T.V. Choudhary, D.W. Goodman, J. Phys. Chem. B 106 (2002) 340–344.
[51] S.K. Singh, Q. Xu, Chem. Commun. 46 (2010) 6545–6547.